Operational Condition and Furnace Geometry for Premixed C_3H_8/Air MILD Combustion of High Thermal-Intensity and Low Emissions

Yi Wang[1, 2, 3], Kin-Pang Cheong[1, *], Junyang Wang[1, 3], Shaotong Liu[1], Yong Hu[4], Minking Chyu[3], Jianchun Mi[5]

[1] *School of Aeronautics and Astronautics, Sichuan University, Chengdu, Sichuan 610065, China*
[2] *Department of Mechanical Engineering, Columbia University, New York, NY 10027, USA*
[3] *Sichuan University - Pittsburgh Institute, Sichuan University, Chengdu, Sichuan 610065, China*
[4] *State Key Laboratory of Fire Science, University of Science and Technology of China, Hefei, Anhui 230027, China*
[5] *College of Engineering, Peking University, Beijing 100871, China*
[*] *Corresponding email: kpcheong@scu.edu.cn*

Abstract

MILD combustion is usually operated at relatively low reactivity, which means low thermal intensity, to achieve uniform temperature field and low emissions of CO and NO_x. Further understanding of its emission characteristics at high thermal intensity condition is required to extend its application. In the present numerical study of premixed C_3H_8/air MILD combustion in a forward-flow cylindrical furnace, different operational conditions (equivalence ratio Φ, and thermal input P_{input}) and furnace geometries (side wall angle α, aspect ratio *AR*) are considered to reveal their correlations with pollutant emissions including CO, NO_x and unburned hydrocarbon (UHC) at thermal intensities up to 1.06 MW/m^3. By adopting reactor network calculation with detailed combustion chemistry, it is found that *AR* plays a notable role in controlling CO, NO_x and UHC emissions, while NO_x emission is insensitive to the variation of side wall angle. Both the CO and UHC emissions are related to the internal recirculation flow, but the impact is determined by the location of the recirculating vortex. Moreover, following the parametric study and NO_x formation analysis with an aggressive strategy, the optimized furnace geometry and operating condition of AR = 5, α = 0° and Φ = 0.6 are obtained to significantly reduce the pollutant emissions by 90% for both C_3H_8 and CH_4 fuels. The present investigation offers valuable insights into the next generation, ultra clean, high thermal intensity MILD combustion.

Keywords

premixed MILD combustion, flameless combustion, recirculation ratio, heat release rate, CO and NO emissions, unburned hydrocarbon (UHC), furnace geometry.

1. Introduction

For the past three decades or so, the MILD (moderate or intense low-oxygen dilution) combustion has been regarded as an advanced combustion technology of high thermal efficiency and low pollution emissions [1] since its successful development based on the exhaust gas recirculation (EGR) technology. Worldwide, extensive research have been focused on the occurrence and emission characteristics of MILD combustion [2–4] to promote its applications to various industries like steelmaking and smelting. It is now well accepted that MILD combustion can be established by recirculating flue gas [4], either internally with aerodynamic control [5–7] or externally with additional piping or flow guiding [1], and the NO emission is significantly reduced comparing to traditional combustion [1]. With the dilution and preheating by the recirculated flue gas, the reaction rate of combustion chemistry reduces, and the temperature rise is lowered so that the local hot and bright spot of the flame front can be eliminated. A volumetric reaction zone is then achieved with almost homogenous temperature and species distributions, where flame fronts are invisible, and flameless combustion is named thereby [1].

Although the NO_x emission of MILD combustion is low enough to meet the criteria or standards of some regulations on pollutant emission, its volumetric combustion intensity, which is usually in several hundred kW/m^3, is insufficient to support its applications in high thermal power systems like gas turbines, boilers and aviation propulsions, which require combustion intensity of MW/m^3 [8]. Raising the intensity of MILD combustion directly will increase the NO_x emission as the thermal formation of NO_x becomes predominant when temperature is above 1600 K [9]. Therefore, it is necessary to explore possible ways of ultra-low emission for MILD combustion to ensure its successful realization at high combustion intensity. Besides, under the context of global warming and atmospheric pollution deterioration, reducing the combustion emissions of NO_x, CO, and unburned hydrocarbons (UHC) will help to mitigate these issues and approach the goals of peak carbon dioxide emissions and carbon neutrality.

To reduce the emissions from MILD combustion, there are several methods that have been

reported in the literature. The common and effective way is to optimize the injection pattern/position of reactants, including premixed [6], non-premixed and staging. Khalil et al. [10] found that, for all their tested premixing modes of MILD combustion, the fully premixed mode provides the lowest CO, NO and UHC emissions. A comparable emission performance was obtained by the partially premixed mode with optimized premixing level and crossflow injection, meanwhile avoiding flame flashback and instability issues in fully premixed combustion. Cheong et al. [11,12] reported that the air-fuel separation distance (*S*) is important for the occurrence and emissions of nonpremixed MILD combustion. When *S* is small, the thermochemical and emission characteristics of nonpremixed mode similar to those of premixed mode. Li et al. [13] and Sharma et al. [14] found that asymmetric injection pattern enhances the internal recirculation and thus a further reduction of NO or CO emission can be realized in their experimental investigations on MILD combustion of liquid or solid fuels, with regard to the conventional symmetric pattern. Staging injection method, which turns the simultaneous injections of fuel and oxidant into sequential injections, is also effective in reducing the emissions from MILD combustion. The MILD combustion of pulverized coal with oxygen-staging was demonstrated in a circulating fluidized bed by Zhu et al. [15], whose NO emission is mitigated by increasing or decreasing the oxygen fraction in the primary/secondary or tertiary stage, respectively. Huang et al. [16] and Sharma et al. [17,18] experimentally investigated the possibility of staging MILD combustion, which shows advantageous potential for the pollutant emission reduction from high intensity combustion chamber such as that of a gas turbine. Particularly, Sharma et al. [17] have realized MILD combustion of liquified petroleum gas whose combustion intensity is 40 $MW/m^3 \cdot atm$. The resulted CO and NO emissions are less than 24 and 3 ppm (at 15% O_2), and the UHC emission is undetectable at the exit of the combustor, which is comparable to the emissions from conventional MILD combustion with an intensity of only several hundred $kW/m^3 \cdot atm$.

Another plausible way is the pressurized MILD combustion. Khalil et al. [19,20] found that the pressure effect on NO emission from MILD combustion mainly depends on the thermal boundary condition. For adiabatic case, NO emission increases with pressure [19,20] while for isothermal furnace boundary, the NO emission is found to decrease with evaluated pressure [20]. Very recently,

by conducting numerical simulations of syngas MILD combustion in a counterflow burner, Shi et al. [21] pointed out that high temperature and low NO emission can be simultaneously achieved at high pressure (> 10 atm). However, Tu et al. [22] found that the high pressure does not further reduce the NO and CO emissions from MILD combustion in a reverse flow furnace with pressure up to 8 atm. Therefore, the emission of MILD combustion at high pressure conditions is still an open question that requires more experimental evidence.

In addition to the methods mentioned above to reduce the emissions from MILD combustion, there are other ways such as the adjustments of inlet conditions including global equivalence ratio, injection momentum and reactant diluent [7,9,21]. Once the operation conditions are determined for a specific MILD combustion case, there is still another way to reduce the pollutant emission, though having been considered less, which is to optimize the furnace design. In the literature, there are different designs of combustion chamber, which are closely related to the flow pattern used to establish MILD combustion. Common designs are cubic or cylindrical chambers, with inlet and outlet in the cross-section plane for forward [11,23–26] or reverse flow [27,28]. Alternatively, cyclonic flow [29–33] can be achieved with inlet in the side surface and outlet in the cross-section center. Tu et al. [34] investigated the impact of furnace shape on the establishment and NO emission of MILD combustion by CFD (computational fluid dynamic) simulation. They revealed that a chamber side wall with large divergence angle (~10°) is preferred for CH_4/air MILD combustion in forward flow furnace, since it results in larger reaction zone and lower NO emission than the tested constant cross-section counterparts, while a large convergence angle might be problematic due to the combustion instability issue. Further investigations are worthy to be conducted to explore the high thermal efficiency and ultra-low emission MILD combustion.

The previous work noted above has stimulated the present study. Specifically, the present numerical simulations are conducted to examine the effect of furnace shape on the pollutant emissions from MILD combustion based on the cylindrical, forward-flow furnace which was operated for the premixed C_3H_8/air MILD combustion [7]. The furnace shape alterations considered include: (1) the convergence/divergence of the side wall and (2) the aspect ratio of furnace (i.e., the

ratio of furnace length to radius). Moreover, the present study also aims to seek and develop the next generation of MILD combustion, with ultra-low emissions of various pollutants (NO_x, CO, and UHC) instead of considering NO_x emission only. The present study may provide a guidance to the optimal furnace design for premixed MILD combustion, even under different application conditions such as high intensity mode of MILD combustion for boilers, engines, and gas turbines.

2. Methods

2.1 Experimental Platform

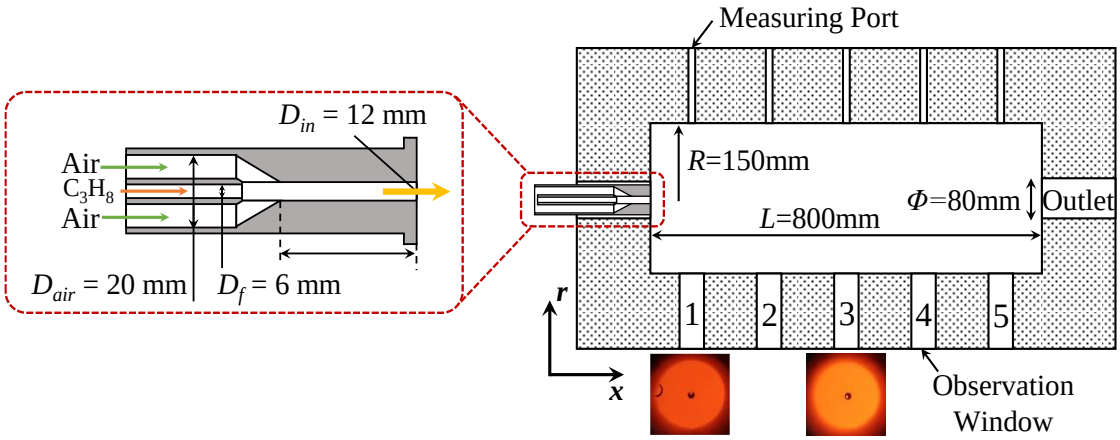

Figure 1 Schematics of the cylindrical MILD combustion furnace and the single jet premixed burner for the present study.

The experimental setup for the premixed propane/air MILD combustion system was detailed in our previous work [7], and only a brief introduction of the burner and chamber is provided here. Figure 1 shows the schematic of the furnace and burner configuration. The physical size of the cylindrical furnace is 300 mm in diameter (D_{fur}) × 800 mm in length (L_{fur}), with the outlet diameter of 80 mm. A series of experiments were conducted for our previous work [7], examining the effects of thermal power input P_{input}, global equavalence ratio Φ, and injection nozzle diameter D_{in}. For the present work investigating the effects of furnace geometry, the operational conditions are fixed as P_{input} = 15 kW, Φ = 0.9, D_{in} = 12 mm. The corresponding injection Reynolds number (Re) of such operation conditions is $Re \approx 30000$. The present CFD modeling is validated by our previous in-furnace measurements of the time-averaged temperature (T) and species (i.e., CO_2, O_2, CO, and NO) concentrations. Readers are referred to our previous study [7] for more details.

2.2 Numerical Setup

The RANS modeling of the MILD combustion is adopted for the present investigations using ANSYS Fluent 16.0 [35], in which the governing equations are detailed. The standard *k-ε* model and EDC (eddy dissipation concept) model are utilized for the encolsures of turbulence equations and turbulence-chemistry interaction, respectively. Although with different values for the constants of the standard *k-ε* and EDC models [36–38], the default ones are selected as we have tested those different values but the improvement is not always positive for different operational condistions [39]. In the present study, reasonable predictions of NO, CO and UHC formations are critical as we need to find out the optimal furnace geometry based on the minimized pollutant emissions by the chamber design. Therefore, several improvements on the numerical setup comparing to our previous study [7] have been carried out: 1) the double precision solver together with stricter convergence criteria, namely 10^{-6} for all unknowns, are applied; 2) the effect of combustion chemistry on the CFD predictions are evaluated by importing global, skeletal and detailed reaction models; 3) additional iterations are continued even when the residuals of temperature and major species concentrations are below 10^{-6} to ensure the variation of outlet NO prediction is less than 1 ppm. Of note, implementing the above will slow down the calculation speed significantly. For compensation, all the simulations are performed in 2D axisymmetric mesh instead of a quarter of the 3D computational domain. The 2D simulation of the current MILD combustion system was proved feasible by Tu et al. [38]. The cell number of the structural 2D mesh is set around 40000 after the independency check with different cell numbers of 15000, 25000, 40000 and 60000. The four tested kinetic models are listed in Table 1, including the global two-step reaction model in Fluent database, a skeletal model proposed by Jiménez et al. [40], the San Diego model (SND) [41] and the USCMech II model (USCMechII) [42] for hydrocarbon fuels. For NO prediction, the reactor network of Fluent is utilized for the cases of two-step and skeletal chemistry, while full simulations of NO formation are performed using SND and USCMechII models with SND and GRI2.11 [43] nitrogen chemistry, respectively. The reactor network model is defined with the following specifications: 1) the detailed mechanism employed was USCGRI and the simulation comprised 1000 reactors after independence check of the reactor

number from 100 to 2000; 2) the numerical integration of the system is performed using a high-precision solver with a relative error tolerance of 1×10^{-5} and an absolute error tolerance of 1×10^{-12}; 3) to enhance computational efficiency and ensuring accurate and reliable results, a segregated solver is selected and the maximum number of iterations allowed for convergence was set to 5000.

Table 1. Summary of the tested combustion chemistry models.

Reaction Model	Combustion chemistry	NO_x chemistry	Species	Reaction steps
USCGRI	The USCMech-II mechanism [42]	GRI2.11 NO_x [43]	111+17	784+102
Skeletal	Skeletal propane mechanism [40]	Reactor network with USCGRI	30	76
SND	The San Diego mechanism [41]	SND NO_x [41]	58+10	269+42

2.3 Model Validations

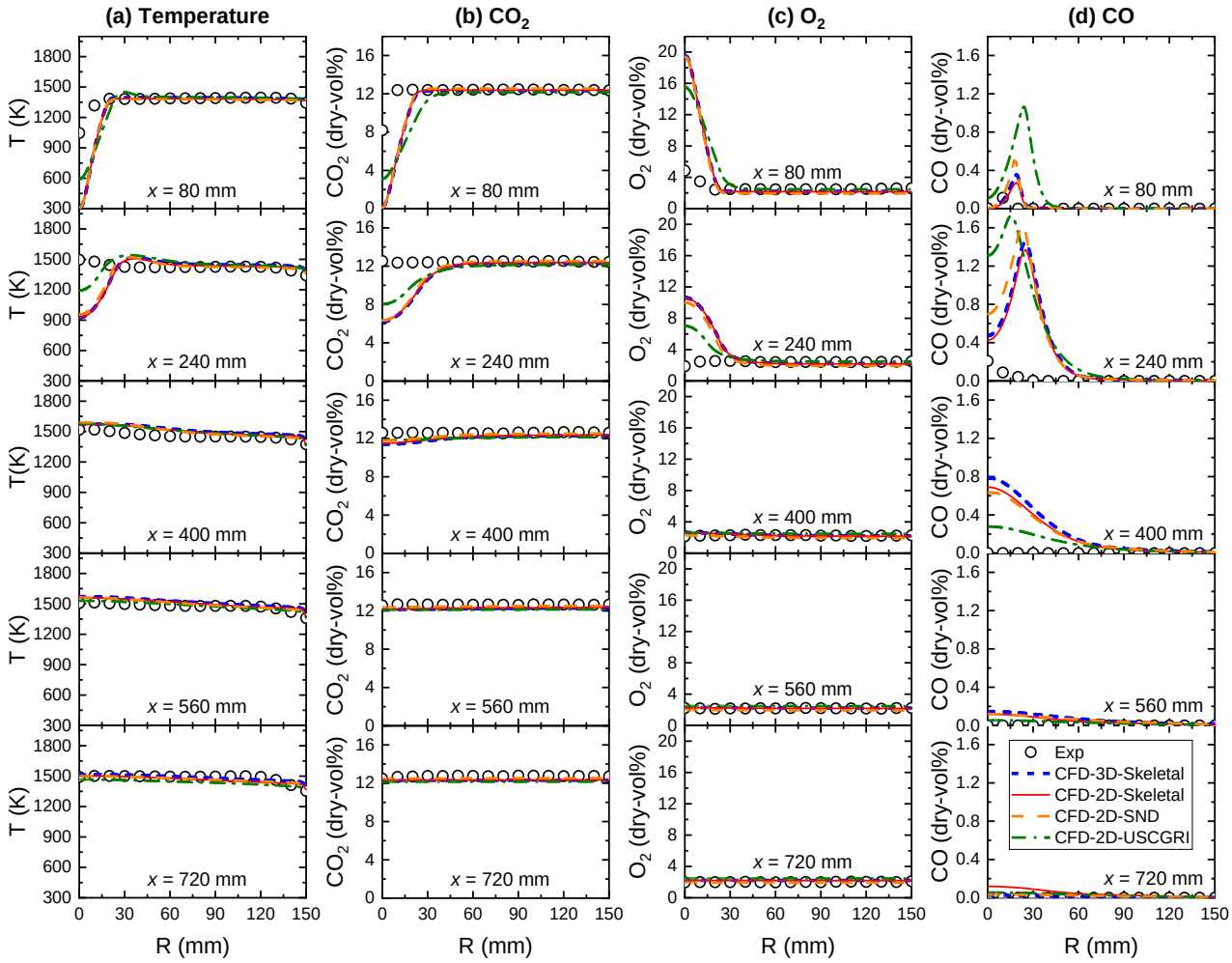

Figure 2 CFD validation for the model setups with different combustion chemistry.

To validate the modeling setup, the predicted results are compared with the in-furnace profiles and emission measurements. Comparisons of radial temperature and species concentration distributions at x = 80, 240, 400, 560 and 800 mm are shown in Fig. 2. It is seen that the present

predictions with 2D axisymmetric computational domain and the skeletal chemistry mechanism is almost identical to those with 3D domain reported in our previous study [7]. This indicates that the simplification of computational domain is suitable for the premixed MILD combustion in a cylindrical furnace with single jet burner. By adopting the SND and USCGRI mechanisms with more detailed combustion chemistry, the predictions near the nozzle located at x = 80 mm and 240 mm can be improved. Also, it appears that better predictions for the CO formation at x = 400-720 mm are provided by USCGRI mechanism.

However, the simulations with the USCGRI mechanism are too computationally expansive even using 2D domain, which requires almost 120 hours to converge for a case in a 48-core workstation. The NO_x post-processing module in Fluent software, which considers simple thermal, prompt, N_2O and reburning routes is also tested. Although it was demonstrated effective in estimating the NO_x emission [34], this module predicts too low, in the order of 0.001 ppmv (not shown here), far from the measured data. Therefore, an alternative method, i.e., the reactor network calculation [44,45], has been applied. The reactor network calculation for NO, CO and UHC analyses using USCGRI mechanism is performed after the simulation with skeletal chemistry mechanism, reducing the required time of convergence to 24 hours with satisfactory accuracy. We assess the validity of the reactor network model as a tool for predicting NO emissions by comparing the NO emissions predicted by the reactor network and the CFD simulation by USCGRI mechanism against the previous measurements [7].

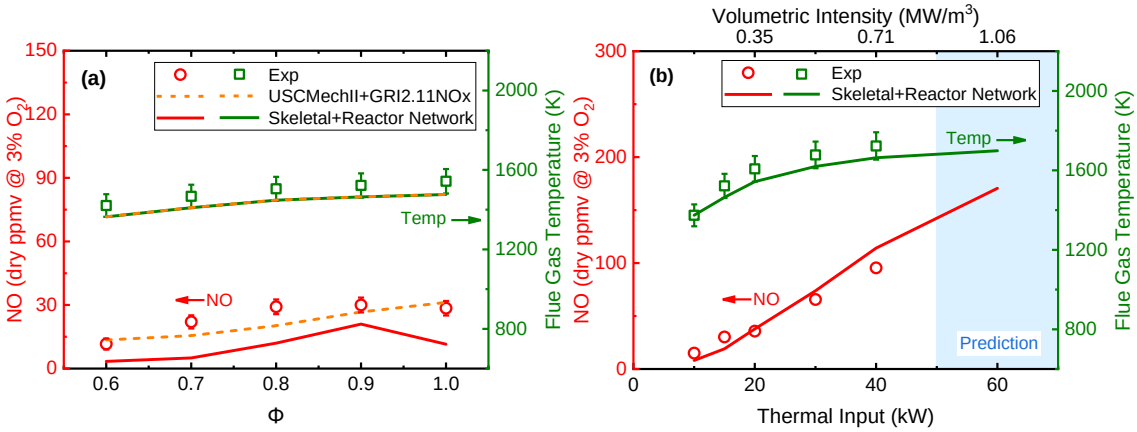

Figure 3 Validation for the present setups using skeletal chemistry and reactor network: (a) varying Φ with P_{input} = 15 kW and (b) varying P_{input} with Φ = 0.9.

Figures 3(a) and 3(b) illustrate the NO emission and flue gas temperature at the outlet (x = 800 mm, R = 0 mm) against the equivalence ratios Φ and thermal input P_{input}. It is demonstrated that the predictions through the USCGRI mechanism agree well with the experimental measurements. This indicates the good performance of USCGRI mechanism though it is too complicated and costly. On the other hand, while more Φ-related deviations from the measurements are seen for the NO emission, the reactor network still correctly predicts the trends of the trends of temperature and NO emissions, as shown in Figs. 3(a) and 3(b). Figure 3(b) further validates the accuracy in NO emission prediction of the current reactor network calculation for different P_{input}, whose uncertainty is generally within 15%. These findings highlight the suitability of the reactor network model as a computationally efficient approach for predicting NO emissions, albeit with some limitations in terms of precision. To the best knowledge of the authors, the present study validates the USCGRI mechanism for NO prediction and reactor network calculation in a laboratory-scale C_3H_8/air MILD combustion furnace for the first time. Figure 3(b) also shows that, as P_{input} increases from 10 kW to 60 kW, the CO and NO emissions increase rapidly and might exceed the emission limits. Therefore, to increase the volumetric intensity of MILD combustion from the order of kW/m^3 (heating furnace) to MW/m^3 (boiler or gas turbine), further considerations in the emission reduction strategy are necessary, which is the motivation of the present study. Hence, the reactor network model is employed herein to evaluate and compare CO, NO and UHC emissions under different geometries so as to obtain the optimal design.

2.4 Alterations of Furnace Geometry

To investigate the effect of furnace geometry on the emissions from MILD combustion, the following alterations have been considered while the thermal input and total volume of the furnace is kept constant in order to compare the emissions under the same thermal intensity: (1) aspect ratio (AR), i.e., length to diameter ratio (LDR) and (2) convergent or divergent side wall as illustrated in Fig. 4, together with the typical meshing of the computational domain. The alterations are summarized in Table 2.

Table 2. Summary of the geometric variances investigated.

Geometric Alteration (constant volume)	**Value**					
Aspect Ratio L_{fur}/D_{fur} (AR)	0.5	1	2	3	4	5
Side wall angle (Divergence [+] or Convergence [-])	+2°	+5°	+10°	-2°	-5°	-10°

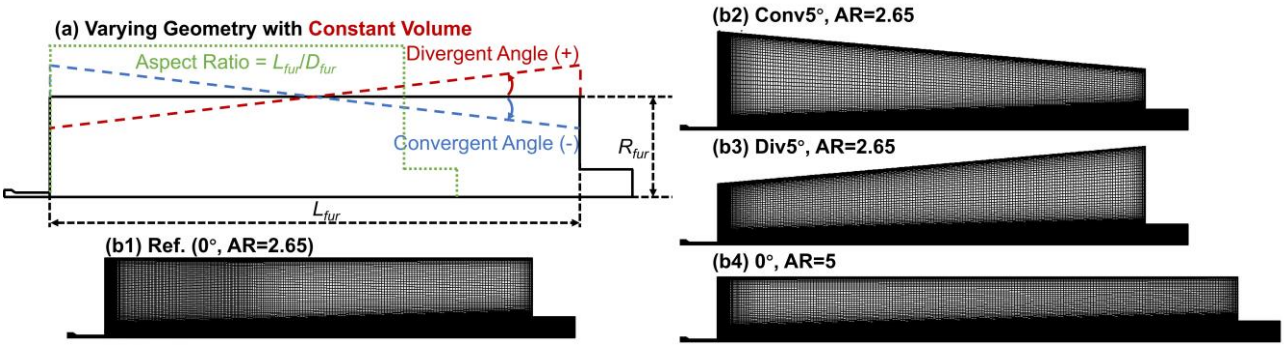

Figure 4 Geometry variations considered in the present study: (a) Schematics of the geometry variations, (b1) - (b4) Representative meshes of different geometry alterations.

In the present study, the entrainment rate or recirculation ratio K_V at any x location can be estimated below viz.:

$$K_V = \frac{M_e}{M_{air} + M_{fuel}} = \frac{M_{x+} - M_{air} - M_{fuel}}{M_{air} + M_{fuel}} \quad (1)$$

In Equ. (1), M_e, M_{fuel} and M_{air} are the mass fluxes of internally entrained flue gas, inlet fuel and air streams, respectively; M_{x+} denotes the mass flow rate of the flow with positive axial velocity.

3. Results and Discussion

The occurrence of MILD combustion can be experimentally determined by the uniformity of chemiluminescence [7,46], while it may be suitably indicated by the distributions of temperature and heat release rate (HRR) for chemical calculations and CFD simulations [12,47]. Moreover, the flue gas recirculation ratio K_V is also considered in the following discussion to reveal the impact of flow on the exhaust emissions from MILD combustion.

3.1 Effects of Operational Conditions

3.1.1 Global equivalence ratio

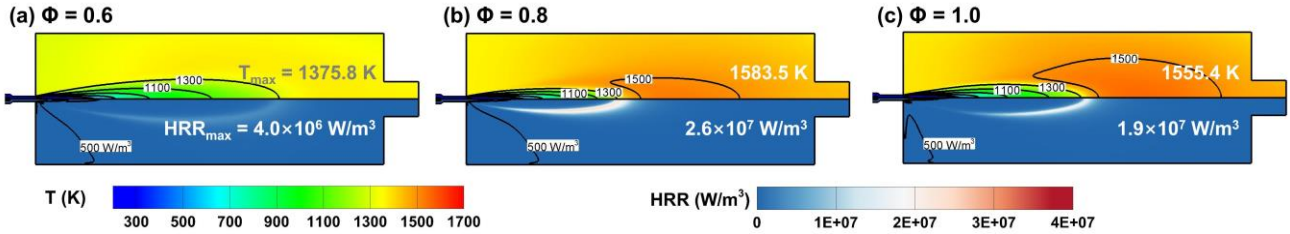

Figure 5 Central-plate mean temperature and HRR distributions for Φ = 0.6, 0.8 and 1.0 at P_{input} = 15 kW.

Figure 5 shows the central-plane mean temperature and HRR contour distributions for Φ = 0.6, 0.8 and 1.0 at P_{input} = 15 kW. Note that both the flow conditions and combustion chemistry are altered by varying Φ, although the flow pattern and flue gas recirculation are still similar [7]. As Φ increases from 0.6 to 0.9 (not shown here), the maxima of the temperature (T_{max}) and HRR (HRR_{max}) rise due to less diluting (room-temperature) air being injected into the furnace and more complete combustion happening under the fuel-lean condition. However, at Φ = 1.0, both T_{max} and HRR_{max} decrease perhaps owing to less oxygen and weaker mixing, resulting in incomplete oxidation and thus less heat release. Moreover, when adopting the isoline of 500 W/m^3 to display the relative volume of heat release or reaction in the furnace, the reaction zone appears to become the most extended at Φ = 1.0. In other words, the reaction zone volume varies inconsistently with the peak temperature and HRR. This implies the importance of balancing the local reactivity and the volume of reaction zone for realizing the volumetric reaction under MILD condition.

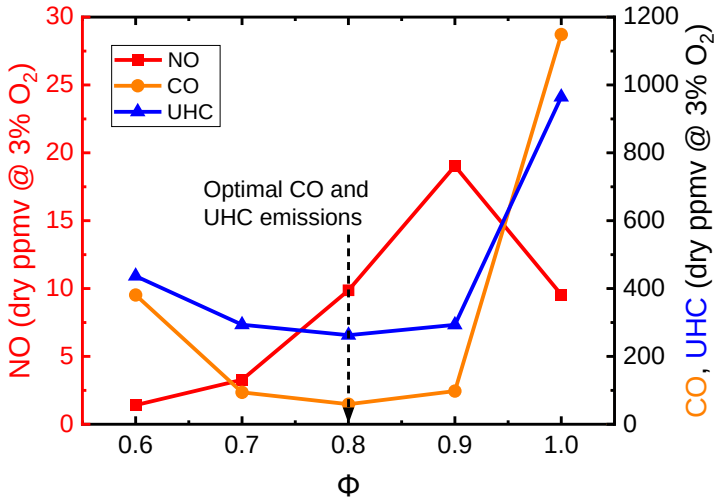

Figure 6 Emissions of NO, CO, and UHC versus Φ for P_{input} = 15 kW.

Figure 6 presents the effects of Φ on the emissions of NO, CO and UHC. Generally, the NO emission should increase with the temperature growth in the reaction zone, while the CO and UHC emissions are related to the fuel burnout. The drop of the NO emission at Φ = 1.0 results from incomplete oxidation (thus reducing atmosphere) and lowered reaction temperature. Particularly, both CO and UHC emissions are over 900 ppmv at Φ = 1.0, increasing dramatically from the case of Φ = 0.9, due to incomplete combustion. For both CO and UHC emissions, the minimum values of 60 ppmv and 260 ppmv are found around Φ = 0.8 and the NO emission peaks at Φ = 0.9, resulting in a preferred Φ around 0.8 to achieve the optimal emissions for the present C_3H_8 MILD combustion. This is consistent with the conclusion of Hu et al. [48] that the optimal Φ for CH_4 MILD combustion is 0.85 based on both CO and NO emissions.

3.1.2 Thermal input

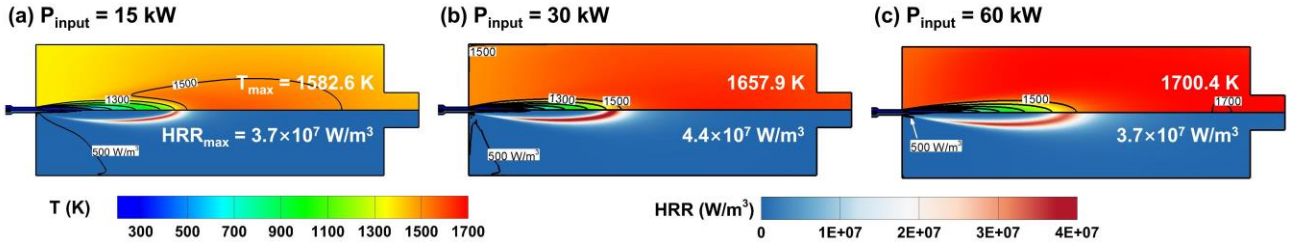

Figure 7 Central-plane mean temperature and HRR distributions for P_{input} = 15, 30 and 60 kW at Φ = 0.9.

To explore the emission characteristics of high intensity MILD combustion, the thermal input of the furnace is varied from P_{input} = 10 kW to P_{input} = 60 kW, correspondingly, the volumetric intensity is increased from 177 kW/m^3 to 1.06 MW/m^3. Figure 7 shows the central-plane mean temperature and HRR contour distributions within the furnace P_{input} = 15, 30 and 60 kW at Φ = 0.9. The approximately uniform temperature distribution with the maximal ΔT < 200 K in the main reaction zone can be observed even at the thermal intensity of 1.06 MW/m^3 (P_{input} = 60 kW), as indicated by the iso-temperature lines in the upper plot parts. Moreover, the iso-line or contour of 500 W/m^3 suggests that almost all the space of the furnace is filled up with the reaction zone for the case of P_{input} = 60 kW. Therefore, it is deduced that MILD combustion can occur at high thermal intensity using the present premixed configuration. Obviously, as P_{input} grows, T_{max} rises (as expected) but

HRR_{max} increases first and then decreases, as shown in Fig. 8. The variation of HRR_{max} may result from the competition between the effects of the flow velocity U and furnace temperature T. By increasing P_{input}, these two factors monotonically increase along but they have adverse impacts on the local reactivity, namely, the suppression by recirculated flue gases and the acceleration by high temperature. If the local reactivity is sufficiently high while with insufficient diluent, the conventional flame front can be formed. Therefore, for high intensity conditions, a large injection velocity may be necessary to increase the recirculation and reduce the local reactivity so that MILD combustion can be established, whose importance has already been claimed by Mi et al. [6] and Veríssimo et al. [49].

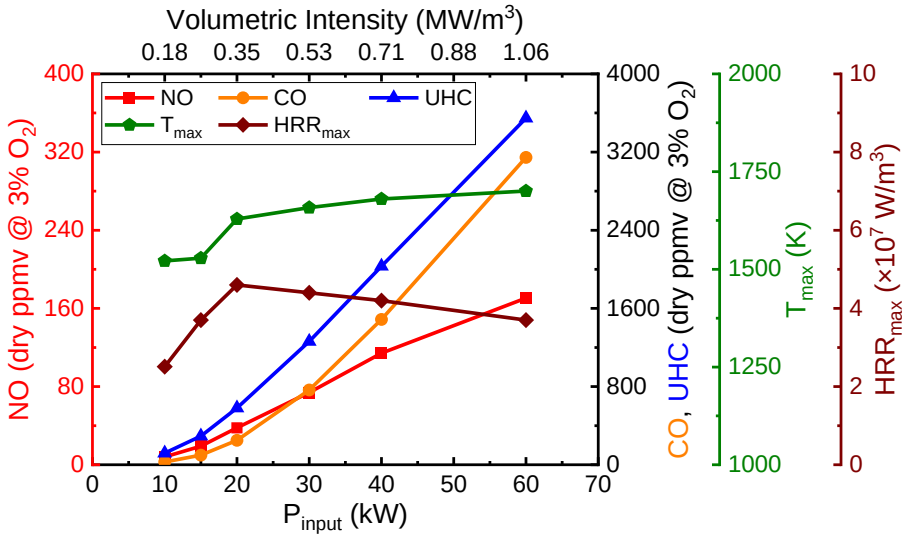

Figure 8 Emissions of NO, CO, and UHC versus P_{input} for Φ = 0.9.

Figure 8 demonstrates that an increase in P_{input} from 10 kW to 60 kW raises all the emissions of NO, CO and UHC dramatically since the volumetric intensity rises. Particularly, a 5-time increment in P_{input} results in an increment in peak temperature of 200 K and a decrement in residence time of 83%, leading to approximate increments of 20-time, 110-time and 30-time for NO, CO and UHC emissions, respectively. The contours of temperature distribution in Figure 7 demonstrate the possibility of high intensity MILD combustion by the present single jet, forward flow, cylindrical furnace, while the plots in Figure 8 simply reveal that the emissions from high intensity MILD combustion may be problematic if no additional optimization in the furnace configuration is taken, which is also the stimulation of the present study.

3.2 Effects of Furnace Geometry

3.2.1 Side wall angle

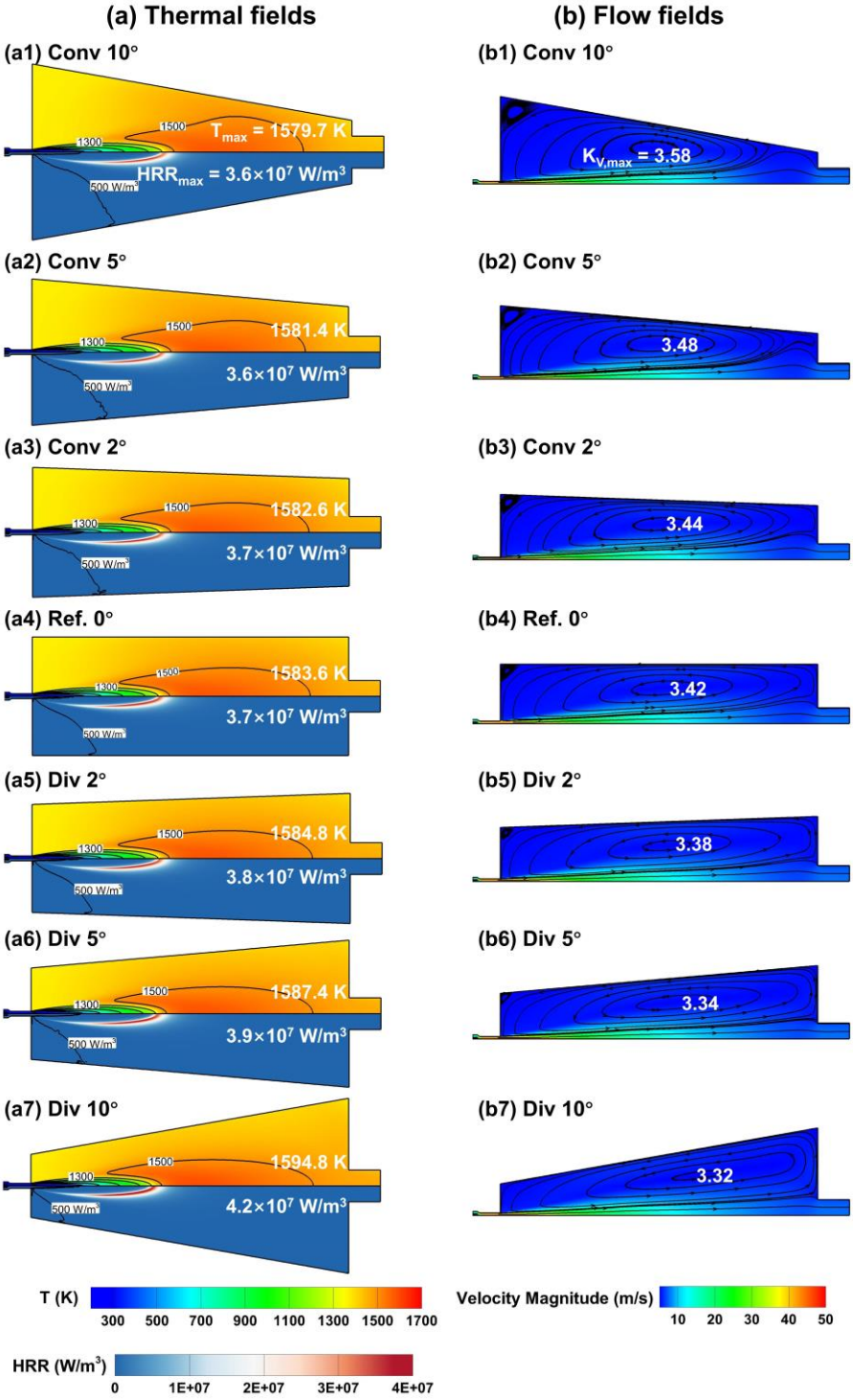

Figure 9 Contour distributions of (a) the mean temperature and heat release rate (HRR) and (b) the mean velocity at various side wall angles (P_{input} = 15 kW, Φ = 0.9).

In Section 3.1, the flow patterns within the furnace at different Φ and P_{input} are found similar so that the flow effect is discussed little there. However, it is expected that the geometry alteration of

furnace will substantially change the flow patterns. It thus follows that the thermal and flow fields are to be both illustrated and analyzed next.

Figure 9 presents the contour distributions of the temperature, HRR and velocity within the furnace at various side wall angles that result in convergent or divergent chamber design. In the convergent series, as the wall angle increases from 0° to 10°, decreases can be observed in the peak values of temperature and HRR, as well as the size of the reaction zone identified by the isoline of HRR = 500 W/m^3. It is implied that a convergent angle reduces the fuel burnout and hence the combustion efficiency. On the other hand, the secondary flow at the corner of the chamber becomes more significant as the convergent angle increases, leading to a larger loss in kinetic energy for the flow. Therefore, the convergent flow design for MILD combustion is not preferential. Conversely, in the divergent series, an increase in the wall angle extends the reaction zone and thus facilitates the occurrence of MILD combustion, consistent with Tu et al. [34]. However, different from the observation of Tu et al. [34], the peak temperature and HRR are also increased with the divergent angle. This is corroborated by the growths in T_{max} from 1584.8 K to 1594.8 K, and HRR_{max} from 3.8×10^7 W/m^3 to 4.2×10^7 W/m^3 as the divergent angle increases from 0° to 10°. These different observations might result from the fuel dependency of MILD combustion on HRR characteristics, as pointed out in our previous work [12], and so a further study is needed.

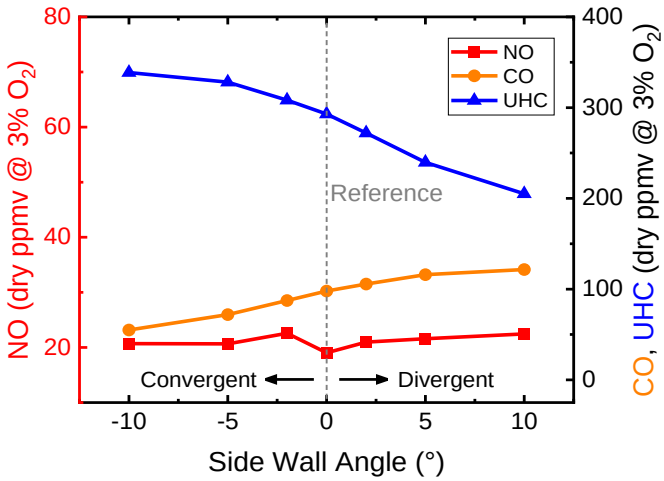

Figure 10 Emissions of CO, NO, and UHC at various side wall angles.

Figure 10 depicts the effects of side wall angle α on the emissions of CO, NO, and UHC from MILD combustion. As α varies from -10° (convergent) to +10° (divergent), the CO emission

decreases from 122 ppmv to 55 ppmv while the UHC emission shows a contrary trend dropping from 338 ppmv to 208 ppmv. It is evident, however, that the NO emission is insensitive to the variation of α. This can be well explained because the stable MILD combustion occurs in all cases of α with uniform distributions of temperature at a nearly identical level. It is worth noting that, if we only consider the emission levels of CO and NO, the convergent design seems to offer more advantages. However, the convergent side wall leads to more UHC emission or incomplete combustion, which is mainly contributed by unburnt H_2 and OH. Hence, multiple emissions should be considered in the design of MILD combustion chamber. A careful inspection of Fig. 9(b) reveals that a convergent side wall shifts upstream the recirculation zone (large-scale vortex) while a divergent side wall shifts it downstream. This is further quantified in Fig. 11(a) since K_V is increased by the wall angle α at x > 400 mm, as K_V represents the rate of recirculation at different side wall angles. The x-location of the maximal rate ($K_{V,max}$) or the vortex center is shown in Fig. 11(b). Also, worth noting is that $K_{V,max}$ slightly reduces with α. Consequently, the convergence increases the emission of UHC whilst the divergence levels up the formation of CO. In other words, it is evident that there is a trade-off between CO and UHC emissions when determining the side wall angle for MILD combustion, in which α = 0° might be an optimal yet conservative choice.

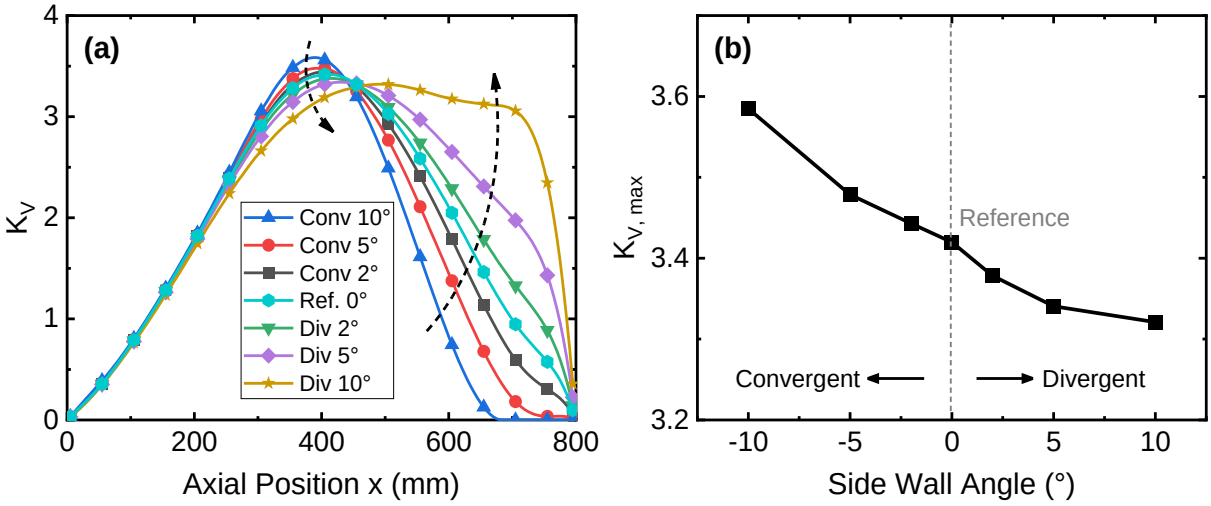

Figure 11 (a) Axial variations of recirculation ratio (K_V) at different values of side wall angle α, and (b) the maximum of K_V versus α, for P_{input} = 15 kW and Φ = 0.9.

3.2 Effects of Aspect Ratio

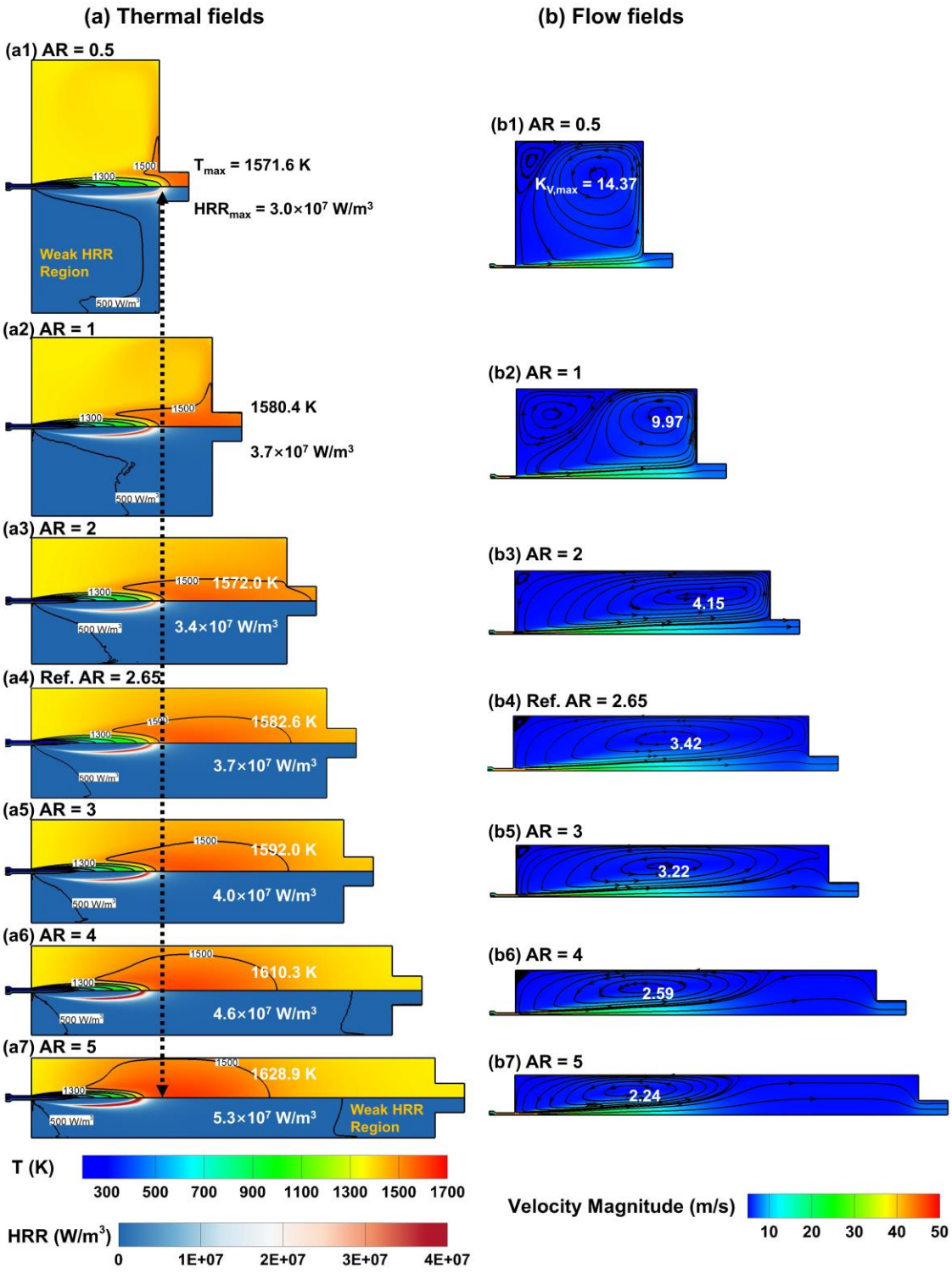

Figure 12 Contour distributions of (a) the mean temperature (T) and heat release rate (HRR) and (b) the mean velocity for AR = 1 to 10 at P_{input} = 15 kW and Φ = 0.9.

Figure 12 shows the center-plane contour distributions of (a) the mean temperature (T) and heat release rate (HRR) and (b) the mean velocity for the aspect ratio AR = 0.5 to 5. The calculations are performed at P_{input} = 15 kW and Φ = 0.9 with constant furnace volume. Specifically, a large AR tends to result in high T_{max} and HRR_{max}, while the volume of reaction zone identified by $HRR \geq 500$ W/m^3,

reaches its maximum at *AR* = 3. On the other hand, the ignition of the premixed reactant is delayed in the cases of small *AR* by the strong dilution of the recirculated flue gas (Figs. 12(b1)-(b3)) and the main reaction zones are cut off due to the short length of the chamber (Figs. 12(a1)-(a3)), which lowers the burnout of the fuel.

As *AR* goes to high values, T_{max} and HRR_{max} also increase with a shrunk reaction zone. This phenomenon can be explained by the closer proximity of the furnace walls to the reactants at higher aspect ratios. The hot furnace walls accelerate ignition and enhance combustion stability through heat radiation. Moreover, when *AR* > 4, a weak HRR region emerges downstream, which is attributed to the accelerated combustion in the upstream region. From the aspect of establishing MILD combustion, *AR* = 3 might be preferred at 15 kW with a large recirculation zone filling up the chamber, as displayed in Figs. 12(b5)-(b6). However, since MILD combustion can be realized at *AR* = 2-5, a furnace with *AR* = 5 can be more compact by saving the volume of weak HRR region without large scale recirculation compared to the furnace with *AR* = 3.

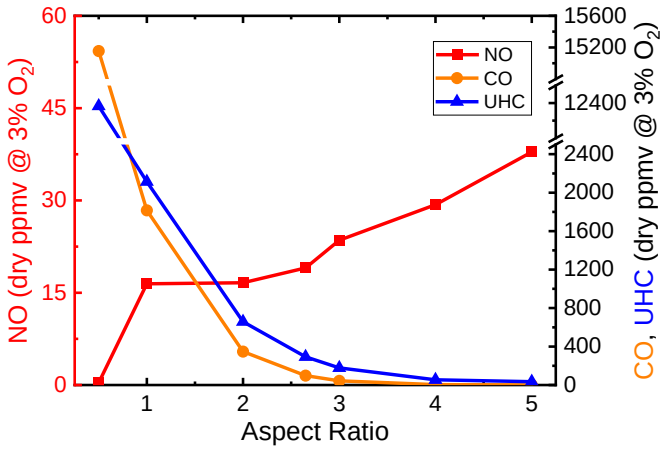

Figure 13 Emissions of CO, NO, UHC versus aspect ratio (*AR*) at P_{input} = 15 kW and Φ = 0.9.

The knowledge learnt from Fig. 12 may be insufficient to determine the optimal *AR*, and, therefore, the emission profiles are further presented in Fig. 13. As *AR* increases, the CO and UHC emissions reduce significantly. For instance, the CO emission decreases drastically from 15154 ppmv at *AR* = 0.5 to 1.6 ppmv at *AR* = 5. Correspondingly, the UHC emission drops from 12366 ppmv to 35 ppmv. In contrast, the NO emission displays an inverse relationship with *AR* due to the rise in T_{max}. Figure 14 shows the variation of K_V with *x* and its peak value against *AR*. Obviously, the

flue gas recirculation rate of mass rises monotonically with *AR*, which facilitates the establishment of MILD combustion. However, the combustion will be incomplete if *AR* is too small. It is interesting to note that, by examining the flow patterns in Fig. 12b and emission profiles in Fig. 13, a large-scale recirculating vortex is beneficial for reducing NO emission (small *AR*), while the non-recirculating forward flow (large *AR*) alleviates the CO and UHC emissions. In summary, *AR* has remarkable effects on the fuel burnout and final exhaust emissions; in the current cases, the balancing of the NO, CO and UHC emissions from MILD combustion concludes that the case of *AR* = 3 represents the optimal choice.

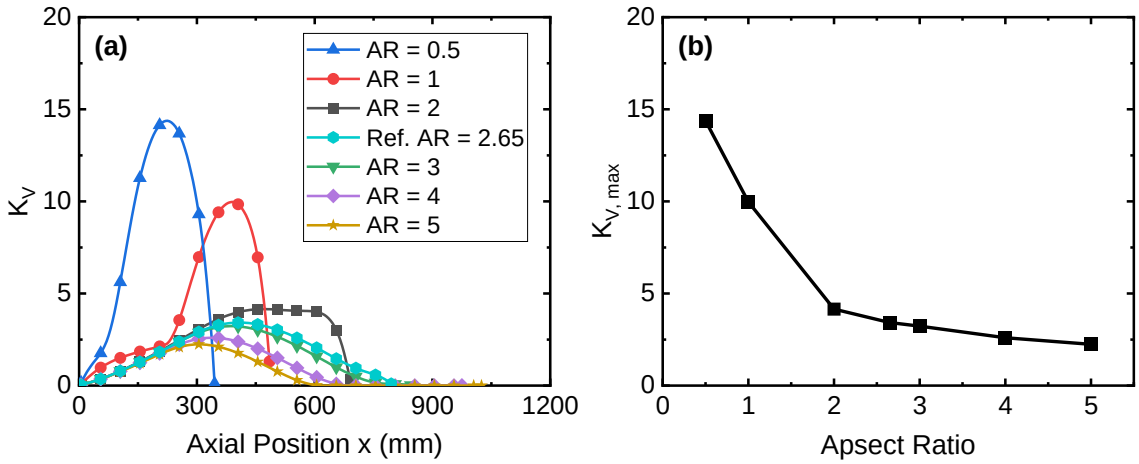

Figure 14 Influence of aspect ratio on K_V (P_{input} = 15 kW, Φ = 0.9).

Overall, the results and discussion presented in Section 3 suggest a complex interplay between geometric design, fluid dynamics, and combustion behavior, which provides important insights for optimizing combustion processes in terms of efficiency, emissions, and operational stability.

4. Further Discussion

4.1 Route Contribution to NO Emission

Some relationships between the furnace configuration and the emissions of NO, CO and UHC have been revealed in Section 3. However, the solution to lower these emissions remains unclear and requires further analysis and discussion on their formation mechanisms, particularly, for NO_x. Therefore, in this section, the individual contributions to the total NO emission from the thermal, prompt, N_2O, and NNH routes as well as NO-reburning are evaluated below, following Cheong et al.

[9] using reactor network calculations with detailed combustion chemistry (see Sections 2.3 and 2.4 for more details).

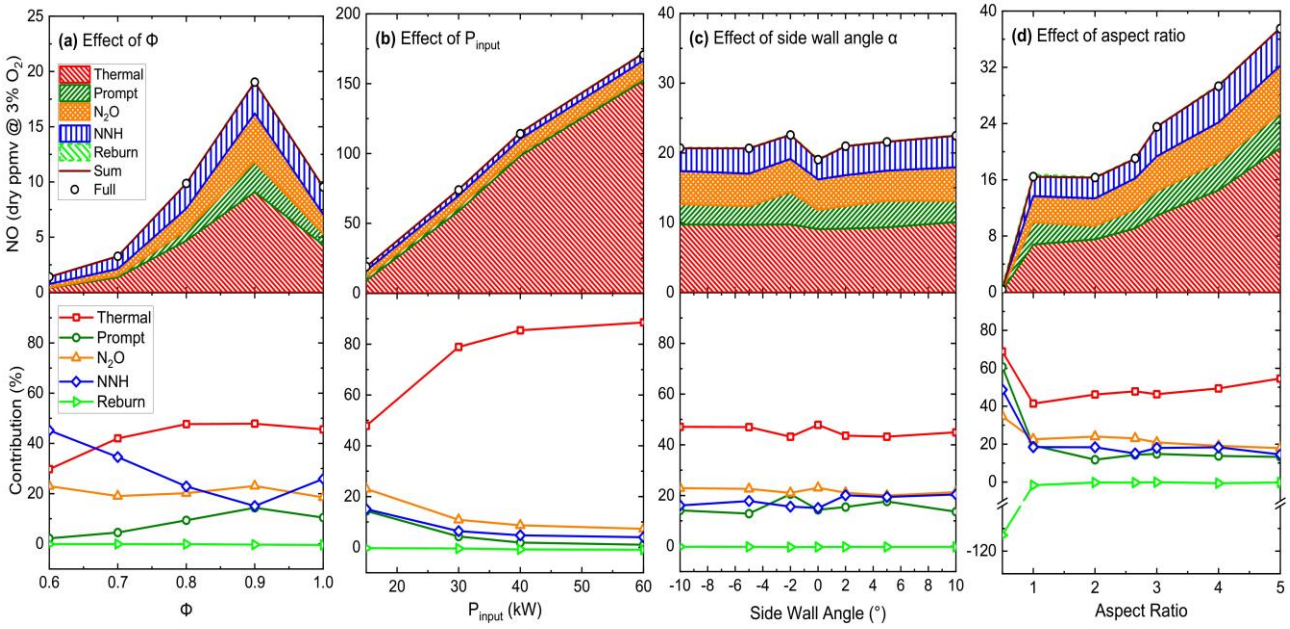

Figure 15 Effects of (a) equivalence ratio Φ, (b) thermal input P_{input}, (c) side wall angle and (d) aspect ratio on the NO contributions from each route.

Figures 15(a)-15(d) show the absolute (upper panel) and relative (lower panel) contributions of NO formation by different routes at various factors discussed in Section 3. Overall, for all the global NO emissions at the outlet of the furnace, the contribution from the reburning is negligible since the it is generally more active at $\Phi > 1.0$ (fuel-rich) and the present cases are all operated at $\Phi < 1.0$ (fuel-lean). Figure. 15(a) demonstrates that the effect of Φ on NO formation is multifold: (1) the temperature rise induced by Φ increases the contribution by the thermal route; (2) the chemical effect of Φ enhances the NO formation via prompt route whilst suppressing the NNH route; (3) the contribution of N_2O route is insensitive to the variation of Φ. For the other factors such as P_{input}, AR, and α, their impacts on the variations in the NO emissions mainly increases the contribution by the thermal route, which is active when the temperature is above 1600 K. Therefore, to effectively reduce the NO emissions at various conditions and furnace design, controlling the furnace temperature, either the average or the peak values, to be less than 1600 K is necessary. Low furnace temperature can be achieved by staged combustion or flue gas quenching, which will be investigated

in the future. Hence, the NO formation analysis in this section offers a practical solution to optimize the NO emission from the present furnace and its design.

4.2 Optimal Furnace Design for High Thermal Intensity MILD Combustion

Table 3. Summary of the geometric variances investigated.

Strategy	Φ	α	*AR*
Reference	0.9	0°	2.65
Optimization 1 (Opt. 1, conservative)	0.8	0°	3
Optimization 2 (Opt. 2, aggressive)	0.6	0°	5

Based on the above findings, the optimal operating conditions and furnace geometry can be determined conservatively by selecting the optimal parameters found in Section 3, i.e., Φ = 0.8, α = 0° and *AR* = 3. However, there is another strategy, which might be aggressive, selecting the extreme conditions for minimizing the emissions of one or a few pollutants instead of balancing all emissions, to counteract the increments induced by other factors. Table 3 lists two strategies for the optimization of the present furnace in terms of pollutant emissions.

Following the conditions listed in Table 2, additional simulations at low and high thermal intensity (15 kW and 60 kW) are performed, and the predicted thermal and flow fields are shown in Fig. 16 with the corresponding emissions plotted in Fig. 17. From Fig. 16, it is confirmed that MILD combustion can be effectively established in these cases with uniform temperature distributions, although their flow patterns are different. By adopting the conservative strategy (Opt. 1), as seen from Fig. 17, noticeable reductions in NO, CO and UHC emissions at low and high thermal intensity (265.3 kW/m^3 and 1.06 MW/m^3) can be obtained, particularly, the CO and UHC emissions can be reduced by over 40%. One the other hand, by adopting the aggressive strategy (Opt. 2), the emission reductions are remarkable, almost over 90% of the pollutants can be removed in the outlet of the furnace comparing to the original design, which is attributed to the factors and mechanisms discussed in Sections 3 and 4.1. In summary, the NO emission is mainly reduced by the low furnace temperature resulting from the small equivalence ratio of Φ = 0.6 and the CO and UHC emissions are alleviated by the non-recirculated forward flow due to the large aspect ratio of *AR* = 5. The

pollutant emissions can be further optimized if the MILD combustion within the furnace can be established over a wide range of conditions. Therefore, the extension of MILD combustion to high thermal intensity applications such as industrial boilers and turbines are very promising, as the wall temperatures of these devices can be lowered by heat extraction and active cooling, together with lean combustion technology to lower the combustion temperature, not only the combustion stability [50] but also the reduction of pollutant emissions can be significantly facilitated. It should also be noted that lean combustion and low combustion temperature may increase the pressure drop induced by injection and reduce the thermal efficiency respectively, which requires further optimization, and the MILD combustion mode should be run at the stage of stable output.

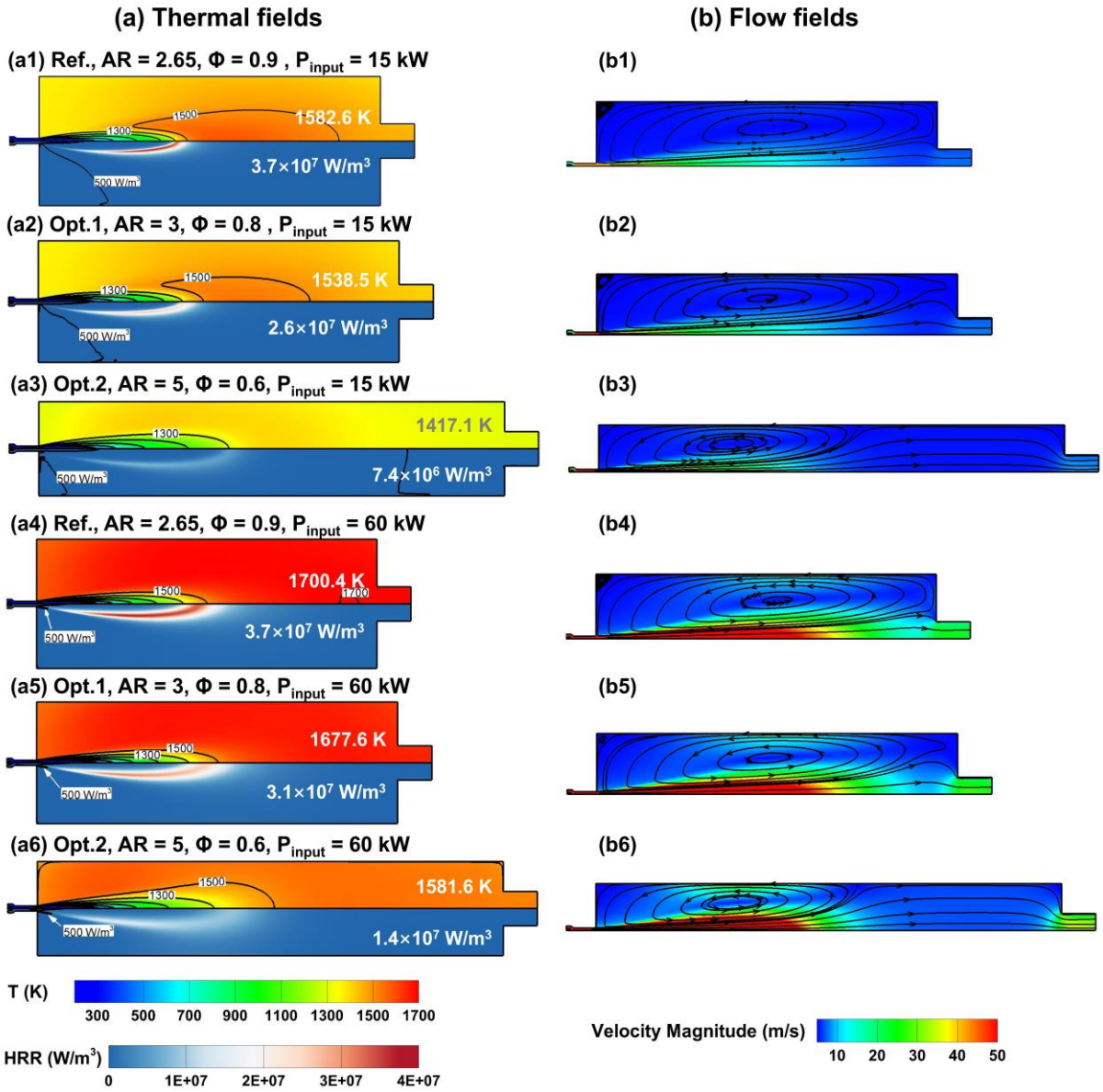

Figure 16 Comparisons of thermal and flow fields between optimized cases and the reference case.

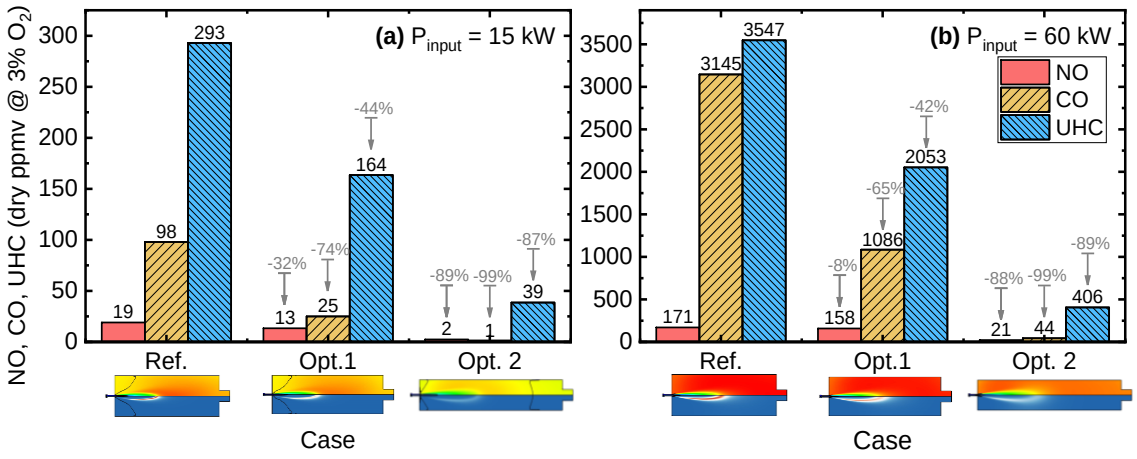

Figure 17 Emissions from optimized cases for premixed C_3H_8/air MILD combustion at: (a) P_{input} = 15 kW, (b) P_{input} = 60 kW.

To further validate the present findings, according to the strategy of Opt. 2, additional simulations are conducted with full GRI2.11 mechanism [43] for the premixed CH_4/air MILD combustion using the same combustion system operated at P_{input} = 60 kW. As clearly shown in Figure 18, the optimized strategy has effectively reduced the NO, CO and UHC emissions from the MILD combustion by over 90%, demonstrating that the present findings are fuel flexible. It is thus concluded that a recirculation zone with a controlled temperature level to suppress NO formation and a followed forward-flow zone to destruct the CO and UHC emissions help to achieve high-intensity, ultra-low emission MILD combustion. Despite the pressure drop and thermal efficiency issues to be addressed for boilers and gas turbines, the present findings could apply to the MILD combustion of heating or kiln furnaces so that the combustion system could be more compact with higher volumetric thermal intensity and even lower pollutant emissions.

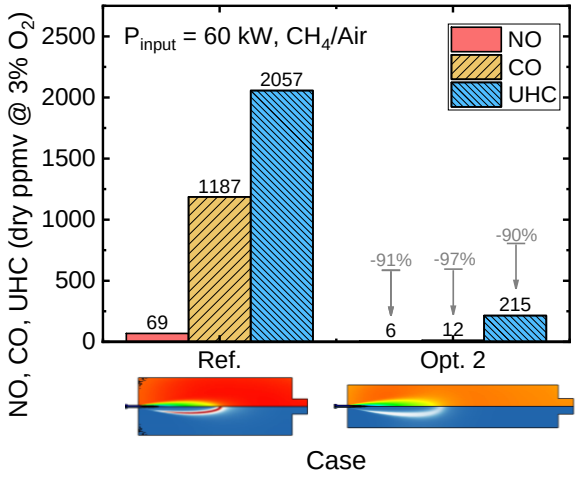

Figure 18 Emissions from optimized cases for premixed CH_4/air MILD combustion P_{input} = 60 kW.

5. Conclusion

This paper presents a comprehensive numerical study of premixed C_3H_8/air MILD combustion in a forward-flow cylindrical furnace to reveal the effects of various operational conditions (equivalence ratio Φ and thermal input P_{input}) and the furnace geometry (side wall angle α and aspect ratio AR) on pollutant emissions for extending the application of MILD combustion to high-intensity power scenarios. The reactor network calculation with detailed combustion chemistry is validated and adopted for the premixed MILD combustion of C_3H_8 for the first time. Based on the effects of the considered factors and the NO contribution analysis, some optimal parameters are successfully obtained for the present MILD combustion furnace. Several main conclusions can be drawn below:

(1) In the optimization of exhaust emissions from C_3H_8/air MILD combustion, assuming similarly for fuels of larger molecules, at least the pollutants of NO, CO and UHC should be considered to reflect the emission level and fuel burnout (or combustion efficiency).

(2) Both CO and UHC emissions from C_3H_8/air MILD combustion reach their minima at $\Phi \approx 0.8$.

(3) The side wall angle imposes a negligible influence on the NO emission but a great impact on both the CO and UHC emissions. Worth noting is that the CO emission is reduced by a convergent side wall while the UHC emission is decreased by a divergent design.

(4) The aspect ratio AR plays an important role in the establishment and emission characteristics of MILD combustion. An increase in AR results in a higher furnace temperature and thus more NO emission but lower CO and UHC emissions. The value of $AR = 6$ is found to be optimal at $P_{input} = 15$ kW when balancing all the emissions.

(5) The CO and UHC emissions are negatively correlated to the intensity of internal flue-gas recirculation (quantified by K_V), and the location of the large-scale vortex influences the CO and UHC emissions.

(6) The parametric study and NO_x formation analysis with an aggressive strategy suggest that almost 90% of the pollutant emissions at both regular and high power intensity conditions

(265.3 kW/m^3 and 1.06 MW/m^3) can be reduced by the optimized furnace geometry and operating condition of AR = 5, α = 0° and Φ = 0.6. This strategy has been further demonstrated in CH_4/air MILD combustion. Hence, lean combustion in a chamber with low operating temperature and large aspect ratio may be a solution for the extension of ultra-clean MILD combustion to high thermal intensity equipment such as boilers and gas turbines.

Conflict of Interest

The authors declare that there are no known conflicts of financial interests or personal relationships that could have appeared to influence the present work.

Acknowledgement

This research is supported by National Natural Science Foundation of China (NSFC) (No. 52006152). K.-P. Cheong also appreciates the support of the Natural Science Foundation of Sichuan Province (No. 2023NSFSC0302).

Nomenclature

Symbols

AR	aspect ratio, the ratio of the length of the furnace to the diameter of the furnace (-)
D_a	diameter of the air nozzle (mm)
D_f	diameter of the fuel nozzle (mm)
D_{fur}	diameter of the furnace (mm)
K_V	internal recirculation rate
L_{fur}	length of the furnace (mm)
M_{air}	mass flow rate of air (kg/s)
M_e	mass flow rate of the entrained flue gas (kg/s)
M_{fuel}	mass flow rate of fuel (kg/s)
M_{x+}	mass flow rate of the flow with positive velocity in x direction (kg/s)
P_{input}	thermal input of the furnace (kW)
R	radial location (mm)
T	temperature (K)
x	axial location (mm)
HRR	heat release rate (W/m^3)

Greek letters

Φ	equivalence ratio
α	side wall angle of the furnace

References

[1] J.A. Wünning, J.G. Wünning, Flameless oxidation to reduce thermal NO-formation, Prog. Energy Combust. Sci. 23 (1997) 81–94. https://doi.org/10.1016/S0360-1285(97)00006-3.

[2] A. Cavaliere, M. de Joannon, Mild combustion, Prog. Energy Combust. Sci. 30 (2004) 329–366.

[3] A.A.V. Perpignan, A. Gangoli Rao, D.J.E.M. Roekaerts, Flameless combustion and its potential towards gas turbines, Prog. Energy Combust. Sci. 69 (2018) 28–62. https://doi.org/10.1016/j.pecs.2018.06.002.

[4] J. Mi, P. Li, F. Wang, K.-P. Cheong, G. Wang, Review on MILD combustion of gaseous fuel: Its definition, ignition, evolution, and emissions, Energy Fuels. 35 (2021) 7572–7607. https://doi.org/10.1021/acs.energyfuels.1c00511.

[5] C. Rottier, C. Lacour, G. Godard, B. Taupin, A.M. Boukhalfa, D. Honoré, An aerodynamic way to reach mild combustion regime in a laboratory-scale furnace, in: THIRD Eur. Combust. Meet., 2007: pp. 1–6.

[6] J. Mi, P. Li, B.B. Dally, R.A. Craig, Importance of initial momentum rate and air-fuel premixing on moderate or intense low oxygen dilution (MILD) combustion in a recuperative furnace, Energy Fuels. 23 (2009) 5349–5356. https://doi.org/10.1021/ef900866v.

[7] K.-P. Cheong, G. Wang, J. Mi, B. Wang, R. Zhu, W. Ren, Premixed MILD combustion of propane in a cylindrical furnace with a single jet burner: combustion and emission characteristics, Energy Fuels. 32 (2018) 8817–8829. https://doi.org/10.1021/acs.energyfuels.8b01587.

[8] J. Ye, P.R. Medwell, E. Varea, S. Kruse, B.B. Dally, H.G. Pitsch, An experimental study on MILD combustion of prevaporised liquid fuels, Appl. Energy. 151 (2015) 93–101. https://doi.org/10.1016/j.apenergy.2015.04.019.

[9] K.-P. Cheong, P. Li, F. Wang, J. Mi, Emissions of NO and CO from counterflow combustion of CH 4 under MILD and oxyfuel conditions, Energy. 124 (2017) 652–664. https://doi.org/10.1016/j.energy.2017.02.083.

[10] A.E.E. Khalil, V.K. Arghode, A.K. Gupta, Novel mixing for ultra-high thermal intensity distributed combustion, Appl. Energy. 105 (2013) 327–334. https://doi.org/10.1016/j.apenergy.2012.12.071.

[11] K.-P. Cheong, G. Wang, B. Wang, R. Zhu, W. Ren, J. Mi, Stability and emission characteristics of nonpremixed MILD combustion from a parallel-jet burner in a cylindrical furnace, Energy. 170 (2019) 1181–1190. https://doi.org/10.1016/j.energy.2018.12.146.

[12] K.-P. Cheong, G. Wang, J. Si, J. Mi, Nonpremixed MILD combustion in a laboratory-scale cylindrical furnace: Occurrence and identification, Energy. 216 (2021) 119295. https://doi.org/10.1016/j.energy.2020.119295.

[13] P. Li, F. Wang, Y. Tu, Z. Mei, J. Zhang, Y. Zheng, H. Liu, Z. Liu, J. Mi, C. Zheng, Moderate or intense low-oxygen dilution oxy-combustion characteristics of light oil and pulverized coal in a pilot-scale furnace, Energy Fuels. 28 (2014) 1524–1535. https://doi.org/10.1021/ef402240w.

[14] S. Sharma, H. Pingulkar, A. Chowdhury, S. Kumar, A new emission reduction approach in MILD combustion through asymmetric fuel injection, Combust. Flame. 193 (2018) 61–75. https://doi.org/10.1016/j.combustflame.2018.03.008.

[15] S.-J. Zhu, Q.-G. Lyu, J.-G. Zhu, J.-R. Li, NO emissions under pulverized char MILD combustion in O_2/CO_2 preheated by a circulating fluidized bed: Effect of oxygen-staging gas distribution, Fuel Process. Technol. 182 (2018) 104–112. https://doi.org/10.1016/j.fuproc.2018.09.002.

[16] M. Huang, R. Li, J. Xu, S. Cheng, H. Deng, Z. Rong, Y. Li, Y. Zhang, Effect of equivalence ratio and staging ratio on the methane MILD combustion in dual-stage combustor, Fuel. 307 (2022) 121903. https://doi.org/10.1016/j.fuel.2021.121903.
[17] S. Sharma, P. Singh, A. Gupta, A. Chowdhury, B. Khandelwal, S. Kumar, Distributed combustion mode in a can-type gas turbine combustor – A numerical and experimental study, Appl. Energy. 277 (2020) 115573. https://doi.org/10.1016/j.apenergy.2020.115573.
[18] S. Sharma, A. Chowdhury, S. Kumar, A novel air injection scheme to achieve MILD combustion in a can-type gas turbine combustor, Energy. 194 (2020) 116819. https://doi.org/10.1016/j.energy.2019.116819.
[19] A.E.E. Khalil, A.K. Gupta, Impact of pressure on high intensity colorless distributed combustion, Fuel. 143 (2015) 334–342. https://doi.org/10.1016/j.fuel.2014.11.061.
[20] H.M. Khalil, Y.A. Eldrainy, W.A. Abdelghaffar, A.A. Abdel-Rahman, Increased heat transfer to sustain flameless combustion under elevated pressure conditions – a numerical study, Eng. Appl. Comput. Fluid Mech. 13 (2019) 782–803. https://doi.org/10.1080/19942060.2019.1645737.
[21] G. Shi, P. Li, F. Hu, Z. Liu, NO mechanisms of syngas MILD combustion diluted with N_2, CO_2, and H_2O, Int. J. Hydrog. Energy. (2022) S0360319922011843. https://doi.org/10.1016/j.ijhydene.2022.03.123.
[22] Y. Tu, S. Xu, M. Xu, H. Liu, W. Yang, Numerical study of methane combustion under moderate or intense low-oxygen dilution regime at elevated pressure conditions up to 8 atm, Energy. 197 (2020) 117158. https://doi.org/10.1016/j.energy.2020.117158.
[23] R. Weber, S. Orsino, N. Lallemant, A. Verlaan, Combustion of natural gas with high-temperature air and large quantities of flue gas, Proc. Combust. Inst. 28 (2000) 1315–1321. https://doi.org/10.1016/S0082-0784(00)80345-8.
[24] R. Weber, J.P. Smart, On the (MILD) combustion of gaseous, liquid, and solid fuels in high temperature preheated air, Proc. Combust. Inst. 30 (2005) 2623–2629.
[25] V.K. Arghode, A.K. Gupta, Investigation of forward flow distributed combustion for gas turbine application, Appl. Energy. 88 (2011) 29–40. https://doi.org/10.1016/j.apenergy.2010.04.030.
[26] V.K. Arghode, A.K. Gupta, K.M. Bryden, High intensity colorless distributed combustion for ultra low emissions and enhanced performance, Appl. Energy. 92 (2012) 822–830. https://doi.org/10.1016/j.apenergy.2011.08.039.
[27] G.G. Szegö, B.B. Dally, G.J. Nathan, Operational characteristics of a parallel jet MILD combustion burner system, Combust. Flame. 156 (2009) 429–438. https://doi.org/10.1016/j.combustflame.2008.08.009.
[28] V.K. Arghode, A.K. Gupta, Investigation of reverse flow distributed combustion for gas turbine application, Appl. Energy. 88 (2011) 1096–1104. https://doi.org/10.1016/j.apenergy.2010.10.039.
[29] A.E.E. Khalil, A.K. Gupta, Distributed swirl combustion for gas turbine application, Appl. Energy. 88 (2011) 4898–4907. https://doi.org/10.1016/j.apenergy.2011.06.051.
[30] A.E.E. Khalil, A.K. Gupta, Swirling distributed combustion for clean energy conversion in gas turbine applications, Appl. Energy. 88 (2011) 3685–3693. https://doi.org/10.1016/j.apenergy.2011.03.048.
[31] M.D. Joannon, P. Sabia, G. Sorrentino, P. Bozza, R. Ragucci, M. de Joannon, P. Sabia, G. Sorrentino, P. Bozza, R. Ragucci, Small size burner combustion stabilization by means of strong cyclonic recirculation, Proc. Combust. Inst. 36 (2017) 3361–3369. https://doi.org/10.1016/j.proci.2016.06.070.
[32] G. Sorrentino, P. Sabia, M. de Joannon, P. Bozza, R. Ragucci, Influence of preheating and thermal power on cyclonic burner characteristics under mild combustion, Fuel. 233 (2018) 207–214. https://doi.org/10.1016/j.fuel.2018.06.049.
[33] G.B. Ariemma, G. Sorrentino, R. Ragucci, M. de Joannon, P. Sabia, Ammonia/Methane combustion: Stability and NOx emissions, Combust. Flame. 241 (2022) 112071. https://doi.org/10.1016/j.combustflame.2022.112071.

[34] Y. Tu, H. Liu, S. Chen, Z. Liu, H. Zhao, C. Zheng, Effects of furnace chamber shape on the MILD combustion of natural gas, Appl. Therm. Eng. 76 (2015) 64–75. https://doi.org/10.1016/j.applthermaleng.2014.11.007.
[35] ANSYS® Fluent, Release 16.0, (2015).
[36] F.C. Christo, B.B. Dally, Modeling turbulent reacting jets issuing into a hot and diluted coflow, Combust. Flame. 142 (2005) 117–129. https://doi.org/10.1016/j.combustflame.2005.03.002.
[37] A. Parente, M.R. Malik, F. Contino, A. Cuoci, B.B. Dally, Extension of the Eddy Dissipation Concept for turbulence/chemistry interactions to MILD combustion, Fuel. 163 (2016) 98–111. https://doi.org/10.1016/j.fuel.2015.09.020.
[38] Y. Tu, S. Xu, M. Xie, Z. Wang, H. Liu, Numerical simulation of propane MILD combustion in a lab-scale cylindrical furnace, Fuel. 290 (2021) 119858. https://doi.org/10.1016/j.fuel.2020.119858.
[39] G. Wang, K.-P. Cheong, J. Si, J. Mi, Nonpremixed Flameless Combustion in a Furnace: Influence of Burner Configuration, Energy Fuels. 35 (2021) 3333–3347. https://doi.org/10.1021/acs.energyfuels.0c03503.
[40] C. Jiménez, B. Cuenot, T. Poinsot, D. Haworth, Numerical simulation and modeling for lean stratified propane-air flames, Combust. Flame. 128 (2002) 1–21. https://doi.org/10.1016/S0010-2180(01)00328-5.
[41] Chemical-Kinetic Mechanisms for Combustion Applications. San Diego Mechanism web page, Mechanical and Aerospace Engineering (Combustion Research), University of California at San Diego. http://web.eng.ucsd.edu/mae/groups/combustion/mechanism.html, 2016 [Last accessed on 16.11.2021].
[42] H. Wang, X. You, A.V. Joshi, S.G. Davis, A. Laskin, F. Egolfopoulos, C.K. Law, USC mech version II. High-temperature combustion reaction model of H_2/CO/C_1-C_4 Compounds. http://ignis.usc.edu/Mechanisms/USC-Mech%20II/USC_Mech%20II.htm, (2007) [Last accessed on 18.10.2019].
[43] C.T. Bowman, R.K. Hanson, D.F. Davidson, W.C. Gardiner Jr, V. Lissianski, G.P. Smith, D.M. Golden, M. Frenklach, M. Goldenberg, GRI-Mech 2.11, [cited 2015 Dec 18]. Available from: http://www.me.berkeley.edu/gri-mech, (1994).
[44] A. Mardani, A. Fazlollahi Ghomshi, Numerical study of oxy-fuel MILD (moderate or intense low-oxygen dilution combustion) combustion for CH_4-H_2 fuel, Energy. 99 (2016) 136–151. https://doi.org/10.1016/j.energy.2016.01.016.
[45] H. Shi, S. Liu, C. Zou, L. Dai, J. Li, W. Xia, J. Yang, J. Luo, W. Li, Experimental study and mechanism analysis of the NOx emissions in the NH_3 MILD combustion by a novel burner, Fuel. 310 (2022) 122417. https://doi.org/10.1016/j.fuel.2021.122417.
[46] P. Li, B.B. Dally, J. Mi, F. Wang, MILD oxy-combustion of gaseous fuels in a laboratory-scale furnace, Combust. Flame. 160 (2013) 933–946. https://doi.org/10.1016/j.combustflame.2013.01.024.
[47] M. de Joannon, G. Sorrentino, A. Cavaliere, MILD combustion in diffusion-controlled regimes of Hot Diluted Fuel, Combust. Flame. 159 (2012) 1832–1839.
[48] F. Hu, P. Li, J. Guo, K. Wang, C. Gong, Z. Liu, New dependence of NO emissions on the equivalence ratio in MILD combustion, Energy Fuels. 32 (2018) 12905–12918. https://doi.org/10.1021/acs.energyfuels.8b02858.
[49] A.S. Veríssimo, A.M.A. Rocha, M. Costa, Importance of the inlet air velocity on the establishment of flameless combustion in a laboratory combustor, Exp. Therm. Fluid Sci. 44 (2013) 75–81.
[50] F. Wang, P. Li, J. Mi, Z. Shu, A novel method to improve stability of MILD combustion in a highly heat-extracted furnace, Fuel. 292 (2021) 120315. https://doi.org/10.1016/j.fuel.2021.120315.